9-13-2013

Mesospheric Hydroxyl Airglow Signatures of Acoustic and Gravity Waves Generated by Transient Tropospheric Forcing

J. B. Snively
Embry-Riddle Aeronautical University, snivelyj@erau.edu

Scholarly Commons Citation

Snively, J. B. (2013), Mesospheric hydroxyl airglow signatures of acoustic and gravity waves generated by transient tropospheric forcing, Geophys. Res. Lett., 40, 4533–4537, doi:10.1002/grl.50886.

GEOPHYSICAL RESEARCH LETTERS, VOL. 40, 4533–4537, doi:10.1002/grl.50886, 2013

Mesospheric hydroxyl airglow signatures of acoustic and gravity waves generated by transient tropospheric forcing

J. B. Snively[1]

Received 11 July 2013; revised 14 August 2013; accepted 16 August 2013; published 13 September 2013.

[1] Numerical model results demonstrate that acoustic waves generated by tropospheric sources may produce cylindrical "concentric ring" signatures in the mesospheric hydroxyl airglow layer. They may arrive as precursors to upward propagating gravity waves, generated simultaneously by the same sources, and produce strong temperature perturbations in the thermosphere above. Transient and short-lived, the acoustic wave airglow intensity and temperature signatures are predicted to be detectable by ground-based airglow imaging systems and may provide new insight into the forcing of the upper atmosphere from below. **Citation:** Snively, J. B. (2013), Mesospheric hydroxyl airglow signatures of acoustic and gravity waves generated by transient tropospheric forcing, *Geophys. Res. Lett.*, *40*, 4533–4537, doi:10.1002/grl.50886.

1. Introduction

[2] Gravity waves exhibiting cylindrical symmetry or curvature have been observed via ground- and space-based imaging systems [*Taylor and Hapgood*, 1988; *Dewan et al.*, 1998; *Sentman et al.*, 2003; *Suzuki et al.*, 2007; *Yue et al.*, 2009, 2013] and clearly correlated with tropospheric convection. Such waves appear in mesospheric and lower thermospheric (MLT) airglow data, exhibiting concentric ring structures, with curvature of the gravity wave phase fronts indicating close proximity to their sources [e.g., *Yue et al.*, 2013].

[3] Numerical 3-D models of tropospheric convection confirm that spatially isolated systems produce gravity waves with cylindrical structure [*Piani et al.*, 2000], which propagate upward into the middle atmosphere. Wave periods of approximately tens of minutes, and wavelengths of approximately tens of kilometers, are excited; exact scales are determined by the characteristics of the system and the state of the tropopause. Ray tracing demonstrates that propagation of such waves is significantly influenced by intervening three-dimensional wind fields [e.g., *Vadas et al.*, 2009], which may result in asymmetry of cylindrical wave structures in the MLT. Existence of multiple simultaneous tropospheric sources may produce superposed concentric gravity wave structures at the heights of the airglow layers [*Vadas et al.*, 2012].

[4] Numerical 2-D cylindrically axisymmetric models reveal gravity wave responses above idealized thermal forcing [*Walterscheid et al.*, 2001]. Infrasonic-acoustic waves are also generated as a response to compressions associated with similar forcing [*Walterscheid et al.*, 2003], with periods of approximately tens of seconds to several minutes, that propagate into the thermosphere. Acoustic and gravity waves are also both reproduced in compressible ray-tracing studies of propagation from simulated convective plumes [e.g., *Vadas*, 2013].

[5] Acoustic waves with periods ∼1–5 min have been identified in the ionosphere above tropospheric convection [e.g., *Georges*, 1973, and references cited therein]. Waves above the Brunt-Väisälä frequency have also been detected in airglow image [e.g., *Hecht et al.*, 2002] and airglow spectral [e.g., *Pilger et al.*, 2013] data, attributable to acoustic, evanescent, or gravity waves (under favorable conditions). Ray tracing of acoustic waves from tropospheric sources suggests amplitudes sufficient to perturb the hydroxyl (OH) layer, which may provide indications of forcing at ground level by various processes [*Bittner et al.*, 2010, and references cited therein]. The observational importance of acoustic waves in the MLT and ionosphere (MLTI) was highlighted following the Tohoku earthquake and tsunami: Acoustic and gravity waves were detected in ionospheric electron density [e.g., *Galvan et al.*, 2011, and references cited therein], and in situ satellite measurements revealed waves in the *F* region, with periods ∼1 min, perturbing neutral density by up to ∼11% with vertical velocities up to ∼130 m/s [*Garcia et al.*, 2013].

[6] The present study aims to provide guidance on the identification of MLT region acoustic waves generated by forcing from below. We investigate, using a numerical model, the observable features of acoustic waves generated by idealized transient tropospheric updrafts and their relationship to simultaneously forced gravity waves. We quantify the integrated intensity and brightness-weighted temperature (BWT) perturbations to the near-infrared (NIR) OH(3,1) emission, which for the modeled waves are estimated to be readily detectable by recent NIR imaging systems [e.g., *Hecht et al.*, 2007; *Taylor et al.*, 2010].

2. Numerical Model Formulation

2.1. Compressible Dynamics and Photochemical Models

[7] Numerical simulations are performed with the nonlinear, compressible, atmospheric model of *Snively and Pasko* [2008], based on the "f-wave" finite volume method of *Bale et al.* [2002] and *LeVeque* [2002], and implemented within the Clawpack software package [http://www.clawpack.org]. The model solves the Euler equations of

[1]Department of Physical Sciences, Embry-Riddle Aeronautical University, Daytona Beach, Florida, USA.

Corresponding author: J. B. Snively, Department of Physical Sciences, Embry-Riddle Aeronautical University, 600 S. Clyde Morris Blvd., Daytona Beach, FL 32114, USA. (snivelyj@erau.edu)

0094-8276/13/10.1002/grl.50886

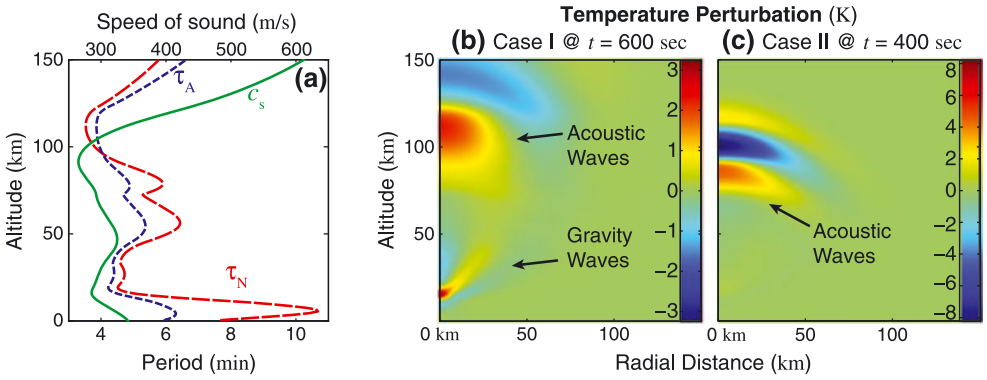

Figure 1. (a) Ambient profiles of sound speed c_s, Brunt-Väisälä period τ_N, and acoustic cutoff period τ_A. Visualization of wave temperature perturbations due to upward propagating acoustic and gravity waves are shown for (b) the Case I source and (c) the Case II source.

conservation of mass, momentum, and energy in a cylindrically axisymmetric domain and supports propagation of steep acoustic waves without formation of artifacts. The domain, with radius r and altitude z, is similar to those of *Walterscheid et al.* [2003] and *de Larquier et al.* [2010]; geometric terms [e.g., *LeVeque*, 2002, pp.433-434] are solved via a second-order approach, using time splitting. Axisymmetric models exclude the influence of winds; however, high-phase-velocity waves are well captured near to their sources.

[8] As only waves with periods on the order of minutes are considered, we include viscosity and thermal conduction but exclude additional absorption processes [e.g., *de Larquier et al.*, 2010]. Viscous terms $\mu\nabla^2\vec{v}$ and $\frac{1}{3}\mu\nabla(\nabla\cdot\vec{v})$ are included in the momentum equation (dynamic viscosity μ varies minimally with altitude, while kinematic viscosity varies with μ/ρ), solved via an explicit method with adaptive time stepping, and applied using a time-split approach [e.g., *Snively and Pasko*, 2008]; conduction is applied similarly. The waves of interest for the present study are not strongly damped below 100 km altitude.

[9] The photochemistry model solves for OH vibrational emissions using the method of *Snively et al.* [2010] for the chemistry of *Adler-Golden* [1997], to obtain perturbed OH(v) densities. Advection equations are solved for N_2, O_2, and O. Full continuity equations are solved for O_3 and H, which include chemical production and loss, and short-lived OH(v) molecules are treated using a steady state approach. We finally calculate the OH(3,1) band-averaged integrated intensity and BWT, which are frequently used in airglow imagery and spectroscopy. Equivalent results (not shown) are also obtained for the (2,0), (4,2), (6,2), and (8,3) bands; due to large vertical wavelengths of acoustic waves, the signatures are not strongly dependent on species layer profiles or peak altitudes.

2.2. Ambient Atmosphere

[10] NRLMSISE-00 temperature and neutral density profiles are specified arbitrarily for 29.2°N latitude, 81.0°W longitude, on 1 January 2010, at 12:00UT [*Hedin*, 1991; *Picone et al.*, 2002]. The waves studied here are not sensitive to specific conditions, and we assume that intervening winds would not strongly influence their upward propagation. The domain extends from 0 to +400 km in the radial r direction and 0 to +400 km in the altitude z direction, with equal dr = dz = 500 m cell dimensions. Open boundaries are placed at r = 400 km and z = 400 km; ground z = 0 km is a reflecting surface. Viscosity and conduction naturally damp waves that propagate vertically toward the upper boundary, and no sponge layer is required [e.g., *Snively and Pasko*, 2008].

[11] Figure 1a depicts profiles of sound speed $c_s=\sqrt{\gamma RT}$, Brunt-Väisälä period $\tau_N = (2\pi)/\omega_N$, where $\omega_N=\sqrt{(g/\theta)(\mathrm{d}\theta/\mathrm{d}z)}$, and acoustic cutoff period $\tau_A = (2\pi)/\omega_A$, where $\omega_A=(c_s/2)(\mathrm{d}(\ln\rho)/\mathrm{d}z)$ [*Gossard and Hooke*, 1975, p.114]. Here γ is the ratio of specific heats, R is the specific gas constant, T is temperature, g is the acceleration of gravity, θ is potential temperature, and ρ is mass density.

2.3. Source Characteristics and Case Studies

[12] Wave sources correspond with single updrafts and subsequent atmospheric responses and are applied via vertical forcing near tropopause. They appear in the momentum equation as a "body force" term [e.g., *Vadas*, 2013], proportional to density, $F_z = \rho A(r,z,t)$. The source is defined by a simple vertical acceleration of Gaussian form $A = A_o \exp[-(r-r_o)^2/2\sigma_r^2 - (z-z_o)^2/2\sigma_z^2 - (t-t_o)^2/2\sigma_t^2]$, where A_o is peak acceleration, σ_r and σ_z are horizontal and vertical half widths (standard deviations), respectively, and σ_t is the temporal half width. The source is positioned at r_o = 0 km and z_o = 12 km, where t_o corresponds to its maximum in time. This form of source differs notably from the oscillatory sources used by *Snively and Pasko* [2008] and *Snively et al.* [2010] to excite gravity waves, near specific periods and wavelengths, with minimal excitation of acoustic waves.

[13] For real convective systems, superposed radiating sources produce a broad spectrum of interacting waves, which propagate in a four-dimensionally varying atmosphere. Case studies here describe only small fractions of realistic spectra, under ideal conditions, and are constructed to illustrate the observable signatures of the waves of interest:

[14] Case study I is specified by σ_r = 5 km, σ_z = 3 km, and σ_t = 60 s, where peak forcing occurs at t_o = 300 s, with amplitude A_o = 0.125 N kg^{-1}. As the full width at half maximum corresponds to a 2.355 min duration, the source excites a spectrum of acoustic and gravity waves near periods τ_A and τ_N. This source is slightly shorter in time scale than the fast "plume" sources investigated by *Vadas* [2013].

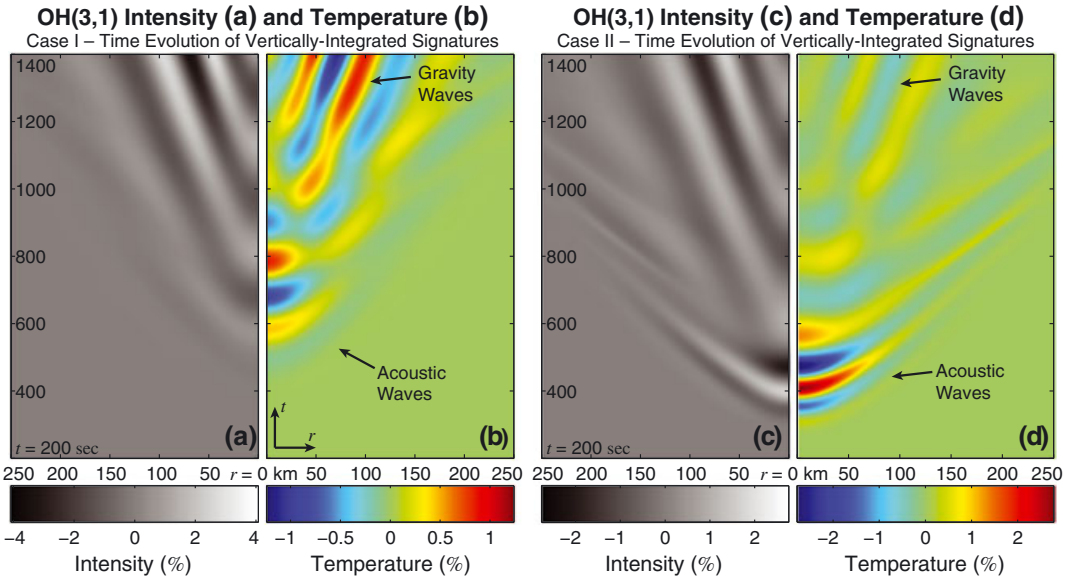

Figure 2. OH airglow (a) intensity and (b) temperature response for Case I forcing and (c) intensity and (d) temperature response for Case II forcing, showing greater acoustic wave intensity.

[15] Case study II is specified by σ_r = 10 km, σ_z= 3 km, and σ_t = 20 s, where peak forcing occurs at t_o= 100 s, with amplitude A_o = 0.04166 N kg^{-1} (resulting in a maximum pressure perturbation ∼1% at its center). As the full width at half maximum corresponds to a short 47.1 s duration, the source is more effective in exciting a spectrum of infrasonic-acoustic waves. Due to its short time scale, its amplitude is reduced by a factor of 3 from Case I. Such a short duration updraft may not be realizable in isolation; it is here used to increase the separation in time scales between gravity and acoustic waves, by more effectively producing acoustic waves at shorter periods.

3. Results

[16] Figure 1b depicts early temperature perturbations for Case I, at simulation time t = 600 s. The more gradual forcing in Case I radiates long period (∼2–4 min), long vertical wavelength (∼50 km), acoustic waves at modest amplitudes of ∼ ±2 K. At later times, the gravity wave response becomes significant. The temperature perturbations by the acoustic waves (not shown) in the thermosphere are approximately tens of kelvin.

[17] Figure 1c depicts early temperature perturbations for Case II, at simulation time t = 400 s. The impulsive forcing produces a stronger acoustic wave response, with MLT temperature perturbations of ∼ ±8 K. As anticipated in section 2.3, the acoustic waves have shorter periods (∼1–2 min) and shorter vertical wavelengths (∼30 km) than those in Case I. Gravity wave perturbations in the stratosphere are initially weak, near the limit of the figure's dynamic range. The larger horizontal scale of the Case II source yields more directive acoustic waves, with less curvature of phase fronts.

[18] Figure 2 illustrates the temporal evolution of OH(3,1) vertically integrated intensity (Figures 2a and 2c) and BWTs (Figures 2b and 2d), here used as a proxy for rotational temperature. Figures 2a and 2b (Case I) reveal similarities in structure and periods of the leading acoustic waves and trailing gravity waves. The acoustic waves are more prominent in the Figures 2c and 2d (Case II), with multiple acoustic oscillations preceding the arrival of the gravity waves. The acoustic waves are refracted and weakly reflected through the MLT and propagate radially outward at greater velocity than the gravity waves.

[19] Figures 3a and 3b illustrate acoustic and gravity wave signatures at r = 0, and the relationship between measured OH intensity and temperature. For Case I (Figure 3a), the modeled airglow signatures reveal ∼3.5 min periodicity of "precursor" acoustic waves, which are followed by the shortest ∼5.5 min gravity waves. The faster source in Case II (Figure 3b) leads to a greater separation between the acoustic waves with period of ∼2 min and gravity waves ∼5.5 min. The transitions between waves are clearest in BWT: the relative temperature perturbations decrease as the gravity wave passes after ∼800 s. Despite carrying significant temperature perturbations (Figure 2d), the acoustic waves produce Krassovsky ratios $((\delta I/\bar{I})/(\delta T/\bar{T}))$ ∼1, i.e., they exhibit temperature and intensity perturbations that are in-phase with similar amplitudes. The gravity waves are more effective than the acoustic waves at perturbing integrated intensity (ratio >1). This is a consequence of the large vertical wavelengths of acoustic waves, which produce opposite perturbations above and below the OH layer peak that "cancel" when integrated vertically [*Snively et al.*, 2010]; off-zenith viewing may thus be beneficial, resulting in reduced cancelation via constructive integration, along certain paths.

[20] Figures 3c–3f depict spatial airglow "images," constructed by interpolating the axisymmetric solutions onto a Cartesian x-y plane. Initial acoustic wave signatures are visibly similar in both Figures 3c and 3e: The acoustic waves form radial "disk" perturbations near the axial centers as they penetrate into the airglow layer. The trailing gravity wave signatures are similar in both cases (Figures 3d and 3f). However, in Case II (Figure 3f), thin concentric rings associated with dispersing acoustic waves are apparent at weak amplitude.

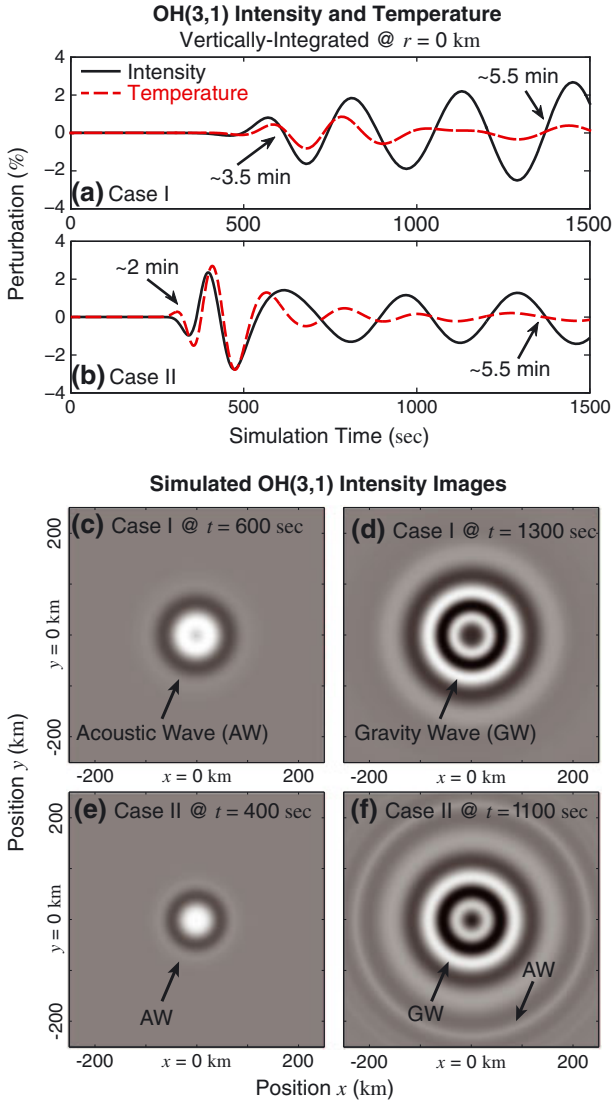

Figure 3. OH airglow intensity and temperature response at $r = 0$, for (a) Case I and (b) Case II, showing acoustic waves preceding the arrival of the highest frequency gravity wave signal. Simulated OH airglow intensity "image," for Case I at (c) early and (d) later times, where acoustic and gravity waves dominate, respectively, and for Case II at (e) early and (f) later times, showing acoustic waves rapidly dispersing away as outer concentric rings surrounding the gravity wave signature.

4. Discussion and Conclusions

[21] For Case I, the more gradual forcing produces acoustic and gravity waves at similar amplitudes and periods. It is hypothesized that similar weak acoustic signatures may exist at detectable amplitude (∼1%) in presently available data, although unambiguous identification may be difficult. For Case II, the more rapid (but less realistic) forcing produces strong acoustic waves at shorter periods ∼2 min. These "precursor" signatures are visibly distinct from the trailing gravity waves and would appear in airglow imagery as a brightening or dimming of a radially-extended region (here ∼75 km radius) prior to onset of concentric ring gravity wave signatures. Confirmation of either event would require identification of acoustic periodicities near the radial center. Acoustic waves may not necessarily arrive prior to gravity waves; indeed, they may be forced intermittently by an evolving storm.

[22] The modeled acoustic wave perturbations are localized and short-lived, detectable only above their sources, and passing within minutes of onset. They are less effective at perturbing vertically integrated OH intensity than gravity waves, yielding small Krassovsky ratios, but sufficiently intense that fast imaging systems [e.g., *Hecht et al.*, 2007; *Taylor et al.*, 2010] may resolve their signatures under favorable conditions. The predicted zenith intensity and temperature perturbations are as large as a few percent of ambient.

[23] Meteorological sources of acoustic waves are not well characterized, such that actual expected amplitudes are not yet known. However, if (or if not) unambiguously identifiable, acoustic waves may provide new insight into the characteristics and evolutions of tropospheric sources and the amplitudes and energetics of acoustic waves in the MLTI above.

[24] **Acknowledgments.** Research was supported by NSF grant AGS-1151746 to Embry-Riddle Aeronautical University. J. B. Snively thanks M. J. Taylor for helpful discussions.

[25] The Editor thanks Edward Llewellyn and an anonymous reviewer for their assistance in evaluating this paper.

References

Adler-Golden, S. (1997), Kinetic parameters for OH nightglow modeling consistent with recent laboratory measurements, *J. Geophys. Res.*, *102* (A9), 19,969–19,976, doi:10.1029/97JA01622.

Bale, D. S., R. J. LeVeque, S. Mitran, and J. A. Rossmanith (2002), A wave propagation method for conservation laws and balance laws with spatially-varying flux functions, *SIAM J. Sci. Comput.*, *24*, 955–978.

Bittner, M., K. Höppner, C. Pilger, and C. Schmidt (2010), Mesopause temperature perturbations caused by infrasonic waves as a potential indicator for the detection of tsunamis and other geohazards, *Nat. Hazards Earth Syst. Sci.*, *10*, 1431–1442, doi:10.5194/nhess-10-1431-2010.

de Larquier, S., V. P. Pasko, H. C. Stenbaek-Nielsen, C. R. Wilson, and J. V. Olson (2010), Finite-difference time-domain modeling of infrasound from pulsating auroras and comparison with recent observations, *Geophys. Res. Lett.*, *37*, L06804, doi:10.1029/2009GL042124.

Dewan, E. M., R. H. Picard, R. R. O'Neil, H. A. Gardiner, J. Gibson, J. D. Mill, E. Richards, M. Kendra, and W. O. Gallery (1998), MSX satellite observations of thunderstorm-generated gravity waves in the mid-wave infrared images of the upper stratosphere, *Geophys. Res. Lett.*, *25*(7), 939–942.

Galvan, D. A., A. Komjathy, M. P. Hickey, and A. J. Mannucci (2011), The 2009 Samoa and 2010 Chile tsunamis as observed in the ionosphere using GPS total electron content, *J. Geophys. Res.*, *116*, A06318, doi:10.1029/2010JA016204.

Garcia, R. F., S. Bruinsma, P. Lognonné, E. Doornbos, and F. Cachoux (2013), GOCE: The first seismometer in orbit around the Earth, *Geophys. Res. Lett.*, *40*, 1015–1020, doi:10.1002/grl.50205.

Georges, T. M. (1973), Infrasound from convective storms: Examining the evidence, *Rev. Geophys. Space Phys.*, *11*(3), 571–594.

Gossard, E. E., and W. H. Hooke (1975), *Waves in the Atmosphere*, Elsevier Scientific, University of Michigan.

Hecht, J. H., R. L. Walterscheid, M. P. Hickey, R. J. Rudy, and A. Z. Liu (2002), An observation of a fast external atmospheric acoustic-gravity wave, *J. Geophys. Res.*, *107*(D20), 4444, doi:10.1029/2001JD001438

Hecht, J. H., A. Z. Liu, R. L. Walterscheid, S. J. Franke, R. J. Rudy, M. J. Taylor, and P.-D. Pautet (2007), Characteristics of short-period wavelike features near 87 km altitude from airglow and lidar observations over Maui, *J. Geophys. Res.*, *112*, D16101, doi:10.1029/2006JD008148.

Hedin, A. E. (1991), Extension of the MSIS thermospheric model into the middle and lower atmosphere, *J. Geophys. Res.*, *96*(A2), 1159–1172.

LeVeque, R. J. (2002), *Finite Volume Methods for Hyperbolic Problems*, Cambridge Univ. Press, Cambridge, U. K.

Piani, C., D. Durran, M. J. Alexander, and J. R. Holton (2000), A numerical study of three-dimensional gravity waves triggered by deep tropical

convection and their role in the dynamics of the QBO, *J. Atmos. Sci.*, *57*(22), 3689–3702.

Picone, J. M., A. E. Hedin, D. P. Drob, and A. C. Aikin (2002), NRLMSISE-00 empirical model of the atmosphere: Statistical comparisons and scientific issues, *J. Geophys. Res.*, *107*(A12), 1468, doi:10.1029/2002JA009430.

Pilger, C., C. Schmidt, and M. Bittner (2013), Statistical analysis of infrasound signatures in airglow observations: Indications for acoustic resonance, *J. Atmos. Solar-Terr. Phys.*, *93*, 70–79.

Sentman, D. D., E. M. Wescott, R. H. Picard, J. R. Winick, H. C. Stenbaek-Nielsen, E. M. Dewan, D. R. Moudry, F. T. São Sabbas, M. J. Heavner, and J. Morrill (2003), Simultaneous observations of mesospheric gravity waves and sprites generated by a midwestern thunderstorm, *J. Atmos. Solar-Terr. Phys.*, *65*, 537–550.

Snively, J. B., and V. P. Pasko (2008), Excitation of ducted gravity waves in the lower thermosphere by tropospheric sources, *J. Geophys. Res.*, *113*, A06303, doi:10.1029/2007JA012693.

Snively, J. B., V. P. Pasko, and M. J. Taylor (2010), OH and OI airglow layer modulation by ducted short-period gravity waves: Effects of trapping altitude, *J. Geophys. Res.*, *115*, A11311, doi:10.1029/2009JA015236.

Suzuki, S., K. Shiokawa, T. Ogawa, K. Nakamura, and T. Nakamura (2007), A concentric gravity wave structure in the mesospheric airglow images, *J. Geophys. Res.*, *112*, D02102, doi:10.1029/2005JD006558.

Taylor, M. J., and H. A. Hapgood (1988), Identification of a thunderstorm as a source of short period gravity waves in the upper atmospheric nightglow emissions, *Planet. Space Sci.*, *36*, 975–985.

Taylor, M. J., P.-D. Pautet, J. Pendleton, R. William, R. Esplin, and D. McLain (2010), Development of an advanced mesospheric temperature mapper (AMTM) for high-latitude research, Abstract C02-0019-10 presented at 38th COSPAR Scientific Assembly, 6 p., Bremen, Germany.

Vadas, S. L. (2013), Compressible *f*-plane solutions to body forces, heatings, and coolings, and application to the primary and secondary gravity waves generated by a deep convective plume, *J. Geophys. Res. Space Physics*, *118*, 2377–2397, doi:10.1002/jgra.50163.

Vadas, S. L., J. Yue, C.-Y. She, P. A. Stamus, and A. Z Liu (2009), A model study of the effects of winds on concentric rings of gravity waves from a convective plume near Fort Collins on 11 May 2004, *J. Geophys. Res.*, *114*, D06103, doi:10.1029/2008JD010753.

Vadas, S. L., J. Yue, and T. Nakamura (2012), Mesospheric concentric gravity waves generated by multiple convective storms over the North American Great Plain, *J. Geophys. Res.*, *117*, D07113, doi:10.1029/2011JD017025.

Walterscheid, R. L., G. Schubert, and D. G. Brinkman (2001), Small-scale gravity waves in the upper mesosphere and lower thermosphere generated by deep tropical convection, *J. Geophys. Res.*, *106*(D23), 31,825–31,832.

Walterscheid, R. L., G. Schubert, and D. G. Brinkman (2003), Acoustic waves in the upper mesosphere and lower thermosphere generated by deep tropical convection, *J. Geophys. Res.*, *108*(A11), 1392, doi:10.1029/2003JA010065.

Yue, J., S. L. Vadas, C.-Y. She, T. Nakamura, S. C. Reising, H.-L. Liu, P. A. Stamus, D. A. Krueger, W. Lyons, and T. Li (2009), Concentric gravity waves in the mesosphere generated by deep convective plumes in the lower atmosphere near Fort Collins, Colorado, *J. Geophys. Res.*, *114*, D06104, doi:10.1029/2008JD011244.

Yue, J., L. Hoffman, and M. J. Alexander (2013), Simultaneous observations of convective gravity waves from a ground-based airglow imager and the AIRS satellite experiment, *J. Geophys. Res. Atmos.*, *118*, 3178–3191, doi:10.1002/jgrd.50341.